Journal of Crystal Growth 383 (2013) 106–111

Contents lists available at ScienceDirect

Journal of Crystal Growth

journal homepage: www.elsevier.com/locate/jcrysgro

Growth of optical-quality, uniform In-rich InGaN films using two-heater metal-organic chemical vapor deposition

S.F. Fu [a], C.Y. Chen [a], F.W. Li [a], C.H. Hsu [a], W.C. Chou [a], W.H. Chang [a], W.K. Chen [a,*], W.C. Ke [b]

[a] Department of Electrophysics, National Chiao Tung University, Hsinchu 300, Taiwan, ROC
[b] Department of Mechanical Engineering, Yuan Ze University, Chung-Li 320, Taiwan, ROC

ARTICLE INFO

Article history:
Received 1 May 2012
Received in revised form
19 June 2013
Accepted 22 July 2013
Communicated by M. Weyers
Available online 2 September 2013

Keywords:
A1. X-ray diffraction
A2. Metal-organic vapor phase epitaxy
B1. Nitrides
B2. Semiconducting indium compounds

ABSTRACT

Good-optical-quality, thick $In_xGa_{1-x}N$ films with high In content were grown using a homemade two-heater metal-organic chemical vapor deposition system. By varying the growth temperature, it was found that the In composition of the InGaN epilayer varied from 18 to 59% as the substrate temperature decreased from 750 to 625 °C. Our results show that the optical properties in terms of the emission peak wavelength and linewidth are uniformly distributed throughout the entire 2 in. wafer for the $x=0.40$ InGaN sample. The resultant mean peak wavelength and FWHM are 808 ± 6 nm and 229 ± 18 meV, respectively, at 18 K. In addition, for the InGaN film grown at 625 °C, a noticeable decrease in the In composition occurred when the ceiling temperature was >800 °C, indicative of the occurrence of parasitic reactions in the gas phase.

1. Introduction

Direct-band-gap $In_xGa_{1-x}N$ alloys have proven to be important materials because of their unique property of wide spectral tunability, which can be adjusted continuously from the ultraviolet through the entire visible region and even extending into the near-infrared region [1–3]. This tunability offers many possibilities in a variety of device applications, including high-brightness visible light emitting diodes (LEDs), laser diodes, full-spectrum multi-junction solar cells and phosphor-free solid-state lighting [1–4]. Despite this peculiar feature, many InGaN studies are presently concerned with Ga-rich alloys, while few attempts have been focused on In-rich $In_xGa_{1-x}N$ ($x>0.30$) with emission wavelengths in the range from the red to the near-infrared region, spanning from 650 to 1100 nm [5–9]. In this region, the light-emission efficiency appears to deteriorate significantly, primarily because of the intrinsic properties of the material itself, such as the wide miscibility gap, the high thermal instability of InN, and the large lattice mismatch between the InGaN emission layer and the GaN base layer, which causes phase separation and compositional fluctuation in the film [10]. The situation is even worse when metal-organic chemical vapor deposition (MOCVD) is employed as the method of film deposition, mainly caused by the use of NH_3 precursor, which is known to have a low cracking efficiency at nominal InGaN growth temperatures (550–800 °C). Several efforts to grow high-quality InGaN films have been put forth by the MOCVD community, including high-growth-rate [11] and raised-pressure methods [12] via either the trapping of In adatoms or the suppression of InN decomposition to increase the In composition. In this study, another approach is proposed. By using a so-called two-heater MOCVD reactor, good-quality In-rich InGaN films of uniform compositional distribution were realized over an entire 2-inch wafer. For example, a sample with $x=0.40$ grown at 650 °C exhibits a mean emission wavelength of 808 ± 6 nm and a mean FWHM of 229 ± 18 meV at 18 K. This suggests that the phase separation and compositional inhomogeneity that are commonly observed in InGaN films in the moderate composition range are suppressed to a great extent at low substrate temperatures by the use of this type of reactor.

2. Experiment

The In-rich $In_xGa_{1-x}N$ epi-films employed here were grown on 2-inch, ~600-nm-thick GaN/(0001) sapphire substrates using a homemade low-pressure horizontal MOCVD reactor equipped with two heating elements, as shown in Fig. 1. One is the substrate heater, which is designed to provide the necessary growth temperature for film deposition; the other is the cracking heater, which is placed on the upper side of the reactor, opposite to the substrate susceptor, for the purpose of providing the ceiling temperature to enhance the supply of active species, especially nitrogen, during the deposition. This arrangement causes the reactor itself to possess the peculiar feature that it is capable of preparing high-In-content InGaN films at low growth

* Correspondence to: Department of Electrophysics, # 1001, Ta Hsueh Rd, Hsinchu 300, Taiwann. Tel.: +886 3 5712121x56125; fax: +886 3 5725230.
E-mail address: wkchen@mail.nctu.edu.tw (W.K. Chen).

0022-0248/$ - see front matter © 2013 Elsevier B.V. All rights reserved.
http://dx.doi.org/10.1016/j.jcrysgro.2013.07.030

temperatures and, most importantly, with fairly good optical properties. In this study, trimethylgallium (TMGa), trimethylindium (TMIn), and ammonia (NH_3) were used as Ga, In and N sources, respectively, and nitrogen was used as the carrier gas. The substrate and ceiling temperatures were monitored by thermocouples inserted into the graphite susceptors. Because of the high thermal conductivity of graphite ($k_{graphite}=53.4$ W/m K), the surface temperature of the substrate is assumed to be nearly the same as the measured thermocouple temperature, based on the calculation of heat transfer by conduction ($\Delta Q/\Delta t = kA\Delta T/\Delta y$). At present, the ceiling temperature cannot be entirely controlled independently because the ceiling temperature alone can heat the substrate susceptor to a certain temperature, which limits the minimum substrate temperature that can be used for film deposition. The resultant InGaN layers were approximately 400 nm thick, as determined by scanning electron microscope (SEM) measurements.

The as-grown epilayers were then examined using an X-ray diffractometer (XRD) in the ω–2θ scan mode of the (002) reflection peak to estimate the In content in the $In_xGa_{1-x}N$ films, under the assumption that Vegard's law is valid. Photoluminescence (PL) measurements were conducted primarily at 14 K using the 325-nm line of a He–Cd laser as an excitation source and a photomultiplier tube or a liquid-nitrogen-cooled extended InGaAs photodiode as a detector. Cathodoluminescence and reciprocal space mapping were also employed to verify the origin of the double luminescence peaks that were exhibited by the high-temperature InGaN films.

3. Results and discussion

The first series of InGaN films were prepared under fixed flow rates of 5.9 and 8.8 μmol/min and 4.8 L/min for TMGa, TMIn and NH_3, respectively, with various substrate and ceiling temperatures being 750, 725, 700, 675, 650 and 625 °C and 1060, 1020, 1010, 945, 900 and 840 °C, respectively. The resultant XRD (002) ω–2θ patterns, scanned from 30.6° to 35.6° and covering the InN and GaN diffraction peaks (31.3° and 34.5°), are shown in Fig. 2(a) and (b). All samples, except the 625 °C sample, appear to exhibit single diffraction peaks. The lack of side diffraction peaks implies that no macroscopic phase separation was present in these samples. The measured In composition, as anticipated, increased from 0.18 to 0.40 as the growth temperature decreased from 750 to 650 °C. The resultant ω–2θ full widths at half maxima (FWHMs) are shown in the inset of Fig. 2(a). Further reducing the growth temperature, although it could increase the In content to 0.59, caused In droplets to form (32.9°), indicating that the In vapor pressure at the growth interface in such a growth environment was above its saturation pressure.

The measured (0002) ω-scan rocking curves at different growth temperatures and the variation of the FWHM as a function of the In content are shown in Fig. 3(a) and (b), respectively. The ω scan is known to represent the orientation spread (crystal mosaicity), which is related to the crystalline quality of the film. It is found that the rocking curve broadens gradually with decreasing growth temperature, i.e., with increasing In content, up to 40%, which can be ascribed in large part to the increased threading dislocation density, composition fluctuation, and large internal strain caused by the difference in interatomic spacing between GaN and InN in the films [13–15]. Further decreasing the growth temperature to 625 °C caused a marked increase of the FWHM in the rocking curve, suggesting that the presence of In droplets caused the film quality to deteriorate significantly.

Fig. 4(a) shows the PL spectra of the above $In_xGa_{1-x}N$ films obtained at 14 K. For the samples grown at temperatures $\geq$ 700 °C, two emission peaks are observable. The corresponding emission peaks, namely, the high- and low-energy emission peaks, are shifted from 2.94 to 2.58 eV and from 2.44 to 2.07 eV, respectively, as the In content increases from 0.18 to 0.30.

The observation of double luminescence peaks in InGaN epilayers has often been attributed to the presence of phase separation and/or strained-relaxed regions [16,17]. The occurrence of macroscopic phase separation can be excluded for our high-temperature films based on the X-ray (002) ω–2θ diffraction profiles, as no additional peak is observed. To verify whether the strain relaxation dominates

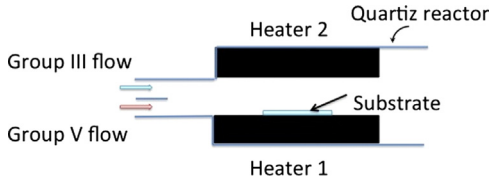

Fig. 1. Cross-sectional sketch of the two-heater MOCVD reactor.

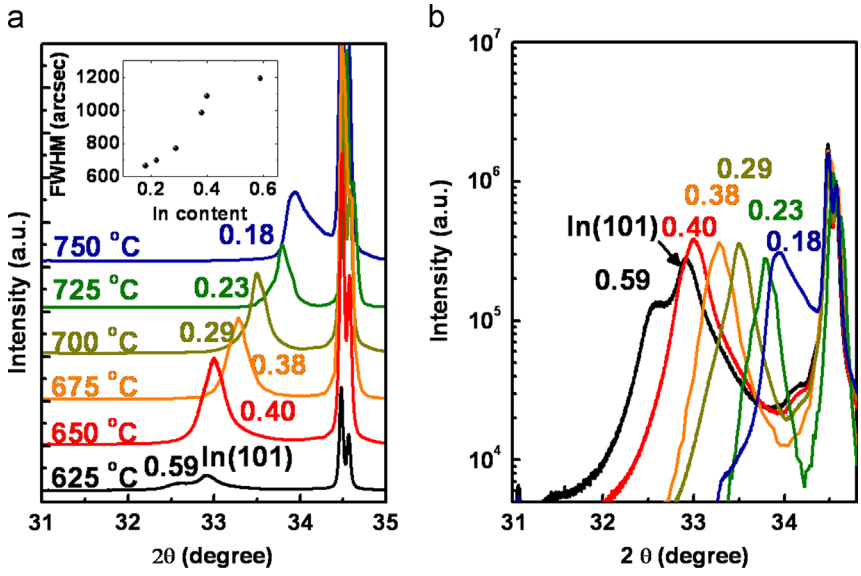

Fig. 2. The XRD (0002) ω–2θ curves of InGaN epilayers grown at various temperatures on (a) linear and (b) logarithmic scales. The corresponding variation in the FWHM as a function of the In content of the films is shown in the inset of (a).

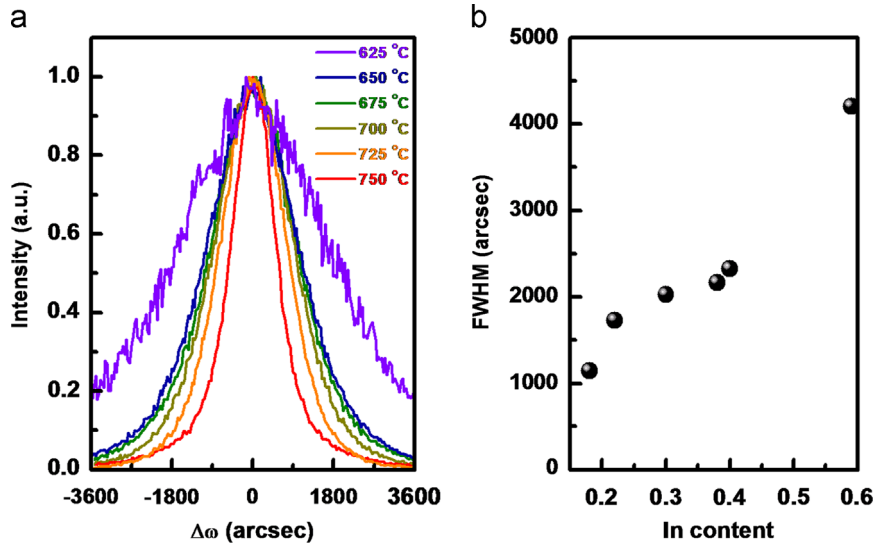

Fig. 3. (a) The XRD (0002) rocking curves of InGaN layers grown at various temperatures and (b) the variation of the FWHM as a function of the In content in the films.

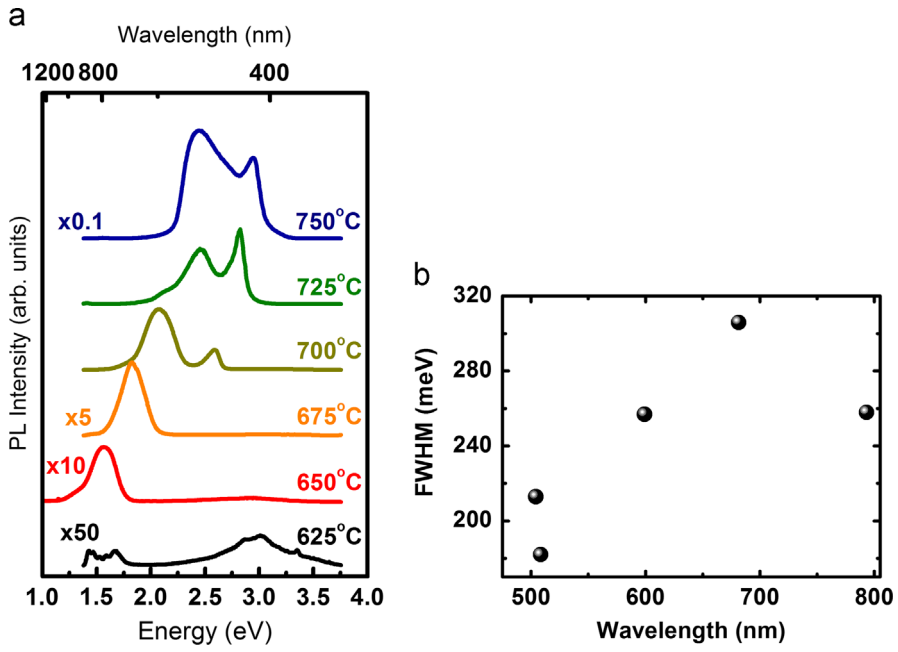

Fig. 4. (a) 14-K PL spectra for InGaN layers grown at various temperatures. (b) Dependence of the FWHM on the emission wavelength for these epilayers.

the luminescent property, we subsequently carried out high-resolution X-ray reciprocal space mapping (RSM), probed at the asymmetrical (105) direction, and cathodoluminescence (CL) measurements on 725 (x=0.23) and 675 °C (x=0.38) samples, which exemplify the characteristics of our high- and low-temperature samples, respectively. From the asymmetrical reflections, both the out-of-plane (c) and in-plane (a) lattice constants can be derived. The resultant RSMs are displayed in Fig. 5(a) and (b). The calculated fully relaxed (dashed) and pseudomorphic (solid) lines are also marked in the figures. As seen, the RSM of the 725 °C sample indeed exhibits two distinct diffraction peaks. One corresponds to a relaxed InGaN region, labeled InGaN(R), and the other is located at a position near the pseudomorphic line, labeled InGaN(S), indicative of the existence of portions of the InGaN region that are coherent with the underlying GaN layer. On the other hand, only a relaxed diffraction peak is observed in the 675 °C sample.

The cathodoluminescence analyses with depth resolution further establish the connection between photoluminescence and the structural properties of the films. By varying the electron-probe beam energy, the luminescence spectra at different depths can be resolved. The resultant CL spectra probed with beam energies varying from 6 to 20 keV, which correspond to depths from the surface of 40 to 500 nm, are presented in Fig. 5(c) and (d). For the 725 °C sample, one can observe from Fig. 5(c) that a low-energy peak at 2.45 eV is promptly excited at the lowest electron energy, while the second high-energy component at 2.82 eV begins to appear at beam energies higher than 8 keV. The depth-dependent CL results clearly indicate that the low-energy component of the 725 °C sample originates from the relaxed region near the surface, whereas the high-energy feature originates from a deeper, strained region, close to the GaN underlayer, which is in good agreement with the results reported by Pereira et al. [17]. The above argument also explains the narrower observed linewidths in the high-energy PL spectra, which are attributable to the improved crystalline quality of the strained region. For the 675 °C sample (x=0.38), only one CL peak is observed, independent of the electron-probe energy, as depicted in Fig. 5(d).

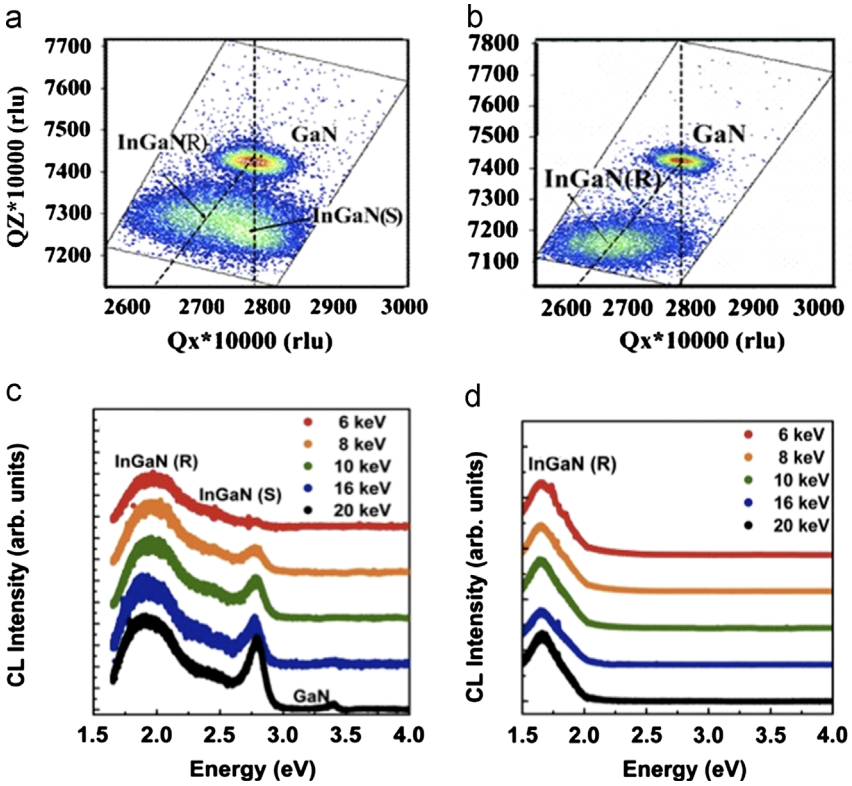

Fig. 5. (105) reciprocal space map of the InGaN epilayers grown at (a) 725 °C and (b) 675 °C; CL spectra acquired at various electron-beam energies for the InGaN epilayers grown at (c) 725 °C and (d) 675 °C.

This finding is also consistent with the result of the RSM measurement, which suggests that the 675 °C film is almost fully relaxed. Such a result could be expected. Because of the increasing lattice misfit, the critical layer thickness of the 675 °C sample ($x=0.38$) on GaN becomes so thin (<3 nm) that the deposition tends to be subjected to an immediate strain relief at the initial growth stage, leaving almost none of the epilayer to remain coherent.

It is worth mentioning that the photoluminescence emission spectra for the $x=0.38$ and 0.40 samples at 14 K peak at 1.82 and 1.68 eV, respectively, corresponding to wavelengths of 681 and 793 nm (854 nm at RT); the latter is well within the infrared color region, which is rarely addressed for thick InGaN layers with high In content by other MOCVD groups. Furthermore, the variation of the linewidths of luminescence peaks from relaxed regions (low-energy components) in these films, obtained from fits with Gaussian functions, is depicted in Fig. 4(b). The resultant linewidth is observed to increase gradually from ~200 to 306 meV with increasing In content, and it becomes narrower, 258 meV, for the InGaN layer of $x=0.4$.

One important concern in this study is the effect of the ceiling temperature on the InGaN growth; we therefore conducted another series of experiments at 625 °C with various ceiling temperatures ranging from 700 to 900 °C. During the growth, the flow rates of TMGa, TMIn and NH_3 were set at 5.9 and 8.8 μmol/min and 5.8 L/min, respectively. No In droplets are observable in this set of samples, which is attributable to the higher NH_3 flow that was employed during the deposition. The In compositions derived from the X-ray data and the PL properties as a function of the ceiling temperature are shown in Fig. 6(a) and (b), respectively. The effects of the ceiling temperature on the InGaN growth are evident. As seen in Fig. 6(a), a slight decrease in the In composition with increasing ceiling temperature is observed at temperatures of 700–800 °C, followed by a steeper fall-off at high temperatures. The PL emission energy essentially reflects the results observed from the X-ray measurement. The emission peak energy remains nearly unshifted in the temperature region of 700–800 °C and rises monotonically as the ceiling temperature is further increased.

For InGaN MOCVD growth, there are two major factors responsible for the decrease of In incorporation; one is In desorption from the growth surface, and the other is parasitic reactions in the gas phase. The reduced In incorporation at high ceiling temperatures can be ascribed to the homogenous gas-phase parasitic reactions that occurred in the high-temperature zone above the susceptor; the substrate temperature of 625 °C that was used here was in the mass-transport-limited growth region (<675 °C), where the desorption of In is insignificant. A detailed explanation is given below.

For nitride MOCVD deposition that involves NH_3 and $(CH_3)_3M$ source precursors, where M=Ga, In or Al, the gas-phase parasitic reactions are generally ascribed to two classes of chemical reactions [18–20]: either the polymerization reactions of group III-ammonia intermediates, such as $(CH_3)_3M{:}NH_3$, $(CH_3)_2MNH_2$, and $(CH_3)MNH$, or the radical recombination reactions of group-III radicals (MCH_3), which are a sequence of dissociation reactions from the intermediates. Unlike AlN, for which the polymerization reactions are initiated at low temperature and exhibit a weak temperature dependence because of the low activation energy, the parasitic reactions of GaN and InN proceed primarily via radical recombination pathways and display steep temperature characteristics, along with a high onset temperature that is necessary to gain sufficient energy to cross the energy barrier and form nuclei and nanoparticle by-products in the gas phase.

The noticeable drop in the In content of our InGaN films at ceiling temperatures >800 °C agrees well with a recent work by Creighton et al. [20]. They reported that near 800 °C, a large portion of the input TMIn reactants are converted into gas-phase metallic In nanoclusters via radical recombination pathways and are no longer available for InGaN deposition because of the

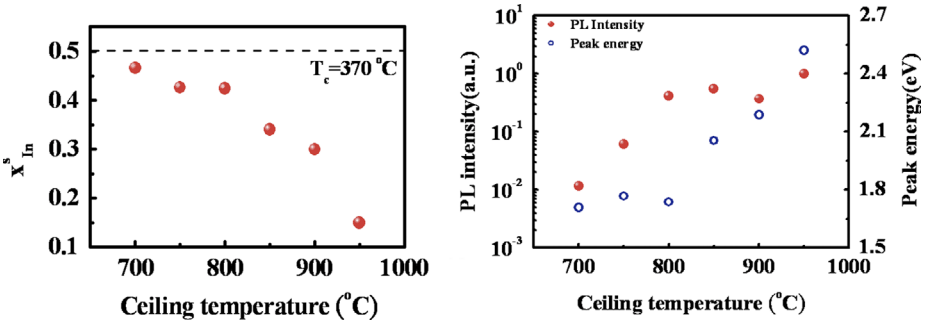

Fig. 6. (a) In composition of the InGaN layer and (b) PL intensity as a function of the ceiling temperature.

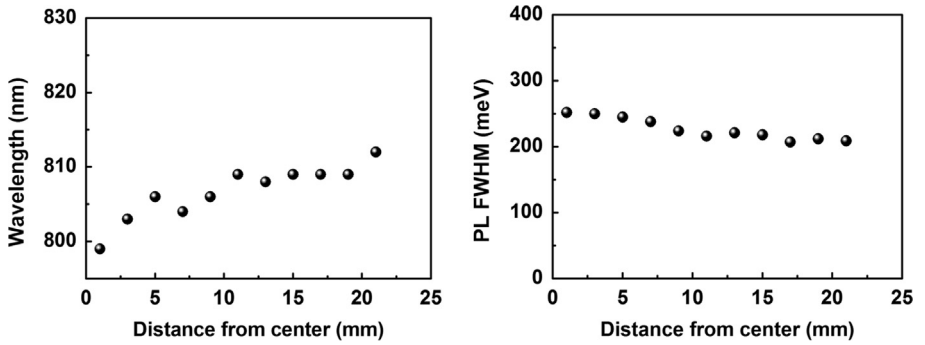

Fig. 7. Wafer-location dependence of the 18-K PL (a) peak wavelength and (b) FWHM for the x=40% InGaN sample.

thermophoretic force near the growth interface. In addition, we find that the PL intensity increases exponentially with the ceiling temperature in the 700–800 °C region. Such a finding suggests that the imposition of a ceiling temperature can indeed exert a positive influence in growing InGaN despite the occurrence of parasitic reactions at high ceiling temperatures.

For the mass production of light-emitting devices, perhaps the most important concern regarding the growth of high-In-content, thick InGaN epilayers is the spectral uniformity over the entire wafer under the influence of an external energy excitation source, such as photon excitation and current injection. To our knowledge, no study has yet been reported concerning the uniformity of the luminescence properties of MOCVD-grown InGaN thick epilayers in the moderate composition range. We therefore focus our discussion on the x=0.40 InGaN sample grown at 650 °C. Fig. 7(a) shows the dependence of the PL peak wavelength at 18 K on the probed position moving from the center toward the periphery of the wafer on a quartered 2-inch wafer. The measured temperature is slightly higher than that used in the PL measurement shown in Fig. 4 simply because of the use of a larger sample size for the sake of uniform measurement. As seen in the figure, good wavelength uniformity is achieved. The PL peak wavelength along the radius fluctuates between 799 and 812 nm throughout most of the wafer area, except for the 2-mm-wide perimeter, where comparatively longer wavelengths are observed because of wafer-edge effects. The deviation of the peak wavelength here is small and comparable to that of the MOCVD-grown undoped InGaN epilayers that emit at a wavelength of ~425 nm [21].

The shift toward longer wavelengths along the radius suggests that more In atoms are incorporated in the film near the periphery of the wafer than at the center. Because the composition of InGaN is sensitive to the growth temperature, the profile of the peak wavelength is closely correlated to the temperature gradient across the wafer. The above result indicates that there was a high-temperature spot of approximately 5 mm in radius located in the central area of wafer, which can be ascribed to the geometric design of our susceptor.

In addition to the PL uniformity, the resultant evolution of the FWHM across the wafer is also depicted in Fig. 7(b). The corresponding PL FWHM varies from 252 to 209 meV, except at the periphery. These values are very narrow compared to the other MOCVD-grown undoped InGaN films (320–400 meV) that emit at infrared colors [22,23] and comparable to those of MBE-grown films [24,25] of a similar wavelength region, where better outcomes were often achieved (216–297 meV).

As mentioned earlier, unlike GaAs and InP material systems, the luminescence spectrum of an In-rich InGaN epilayer is the collective result of light emissions from a large number of In-rich clusters with various sizes, compositions and densities, rather than from the matrix [26]. When the sample is pumped, the excited carriers, created by absorption in the matrix, can diffuse toward and fill up the lower-band-gap, In-rich clusters, yielding photons with energies lower than the band gap of the matrix. This results in a large Stokes shift for the InGaN material [27,28]. Thus, the resultant FWHM of the luminescence peak could resemble, to a certain extent, the distribution of these In-rich clusters, particularly for those of the highest In content. Usually, a rather broader luminescence FWHM is observed for $In_xGa_{1-x}N$ samples when x is close to 0.5, as a significant deviation in composition can occur with a modulation wavelength at a length scale of as little as a few nanometers [14,15]. This is because the film exhibits pronounced lateral decomposition induced by the onset of 3D growth and the generation of misfit dislocations because of strain relaxation, which occurs almost immediately when InGaN is deposited on GaN because of the large lattice mismatch between the two materials [29,30].

Thus, the comparatively narrow FWHM of the luminescence peak for the x=0.40 InGaN sample can be regarded as a signature of the suppression of In aggregation during the deposition. Such a suppression can be attributed primarily to the low deposition

temperature employed in this study, which froze the surface adatoms in areas near the reactant impinging sites and drove the growth conditions away from thermodynamic equilibrium. Consequently, a more uniform In-rich InGaN film was obtained.

Aside from the low deposition temperature, the enhanced supply of active species, particularly the nitrogen in the reactor resulting from the use of the upper heater, may have played a role, as well. This argument is supported by the work of Oliver et al. [31], who, in their study of growth modes in InGaN/GaN heteroepitaxy, suggest that the surface diffusion of group-III adatoms could be hampered by increasing the supply of active nitrogen species, which reduces the barrier for adatom incorporation. This will, in turn, minimize the aggregation of In adatoms at the growth layer, reduce the size and compositional fluctuation of In clusters, and thereby lead to a narrower PL linewidth in the film [32].

4. Conclusions

In summary, we have demonstrated the possibility of growing good-optical-quality, thick InGaN films with high In content using a MOCVD reactor equipped with two heating elements. It is found that by the employment of an additional heater placed on the ceiling of the deposition zone, thick InGaN films of fairly good optical quality can be fabricated with emission wavelengths extending into the infrared region. More importantly, the imposition of a ceiling temperature does not appear to adversely affect the uniformity of the optical properties of the films. For example, an $x=0.40$ InGaN sample grown at 650 °C with a ceiling temperature of 900 °C exhibits a mean emission wavelength of 808 ± 6 nm and a mean FWHM of 229 ± 18 meV at 18 K over the entire 2-inch-diameter substrate. Furthermore, a marked drop-off in In composition for the InGaN film grown at 625 °C is observed when the ceiling temperature is higher than 800 °C, indicative of the occurrence of parasitic reactions in the gas phase in this temperature regime, which deplete the supply of In reactants on the growth surface.

Acknowledgments

This work is supported in part by the projects of MOE-ATU and the National Science Council of Taiwan under Grant no. NSC100-2112-M-009-020-MY3.

References

[1] J. Wu, W. Walukiewicz, K.M. Yu, J.W. Ager III, E.E. Haller, H. Lu, W.J. Schaff, Applied Physics Letters 80 (2002) 4741.
[2] S. Nakamura, G. Fasol, The Blue Laser Diode, Springer, Berlin, 1997.
[3] R.W. Martin, P.R. Edwards, R. Pecharroman-Gallego, C. Liu, C.J. Deatcher, I.M. Watson, K.P. O'Donnell, Journal of Physics D: Applied Physics 35 (2002) 604.
[4] M.G. Craford, Journal of Light and Visual Environment 32 (2008) 58.
[5] X.L. Zhu, L.W. Guo, B.H. Ge, M.Z. Peng, N.S. Yu, J.F. Yan, J. Zhang, H.Q. Jia, H. Chen, J.M. Zhou, Applied Physics Letters 91 (2007) 172110.
[6] V. Gorge, Z. Djebbour, A. Migan-Dubois, C. Pareige, C. Longeaud, K. Pantzas, T. Moudakir, S. Gautier, G. Orsal, P.L. Voss, A. Ougazzaden, Applied Physics Letters 99 (2011) 062113.
[7] B.N. Pantha, J. Li, J.Y. Lin, H.X. Jiang, Applied Physics Letters 93 (2008) 182107.
[8] M. Moret, B. Gil, S. Ruffenach, O. Briot, Ch. Giesen, M. Heuken, S. Rushworth, T. Leese, M. Succi, Journal of Crystal Growth 311 (2009) 2795.
[9] S.C. Bayliss, P. Demeester, I. Fletcher, R.W. Martin, P.G. Middleton, I. Moerman, K.P. O'Donnell, A. Sapelkin, C. Trager-Cowan, W. Van Der Stricht, C. Young, Materials Science and Engineering B 59 (1999) 292.
[10] I. Ho, G.B. Stringfellow, Applied Physics Letters 69 (1996) 2701.
[11] B.N. Pantha, J. Li, H.X. Jiang, Applied Physics Letters 96 (2010) 232105.
[12] D. Iida, K. Nagata, T. Makino, M. Iwaya, S. Kamiyama, H. Amano, I. Akasaki, A. Bandoh, T. Udagawa, Applied Physics Express 3 (2010) 075601.
[13] B.N. Panth, H. Wang, N. Khan, J.Y. Lin, H.X. Jiang, Physical Review B 84 (2011) 075327.
[14] M. Müller, G.D.W. Smith, B. Gault, C.R.M. Grovenor, Acta Materialia 60 (2012) 4277.
[15] T.P. Bartel, P. Specht, J.C. Ho and C. Kisielowski, Philosophical Magazine 87 (2007) 1983.
[16] P. Chen, S.J. Chua, Z.L. Miao, Journal of Applied Physics 93 (2003) 2507.
[17] S. Pereira, M.R. Correia, E. Pereira, C. Trager-Cowan, F. Sweeney, K.P. O'Donnell, E. Alves, N. Franco, A.D. Sequeira, Applied Physics Letters 81 (2002) 1207.
[18] J.R. Creighton, G.T. Wang, W.G. Breiland, M.E. Coltrin, Journal of Crystal Growth 261 (2004) 204.
[19] A.Y. Timoshkin, H.F. Schaefer III, Journal of Physical Chemistry C 112 (2008) 13816.
[20] J.R. Creighton, M.E. Coltrin, J.J. Figiel, Applied Physics Letters 93 (2008) 171906.
[21] M. Bosi, R. Fornari, S. Scardova, M. Avella, O. Martínez, J. Jimenez, Semiconductor Science and Technology 19 (2004) 147.
[22] K.P. O'Donnell, R.W. Martin, S. Pereira, A. Bangura, M.E. White, W. van Der Stricht, K. Jacobs, Physica Status Solidi (b) 216 (1999) 141.
[23] D. Queren, M. Schillgalies, A. Avramescu, G. Brüderl, A. Laubsch, S. Lutgen, U. Strauß, Journal of Crystal Growth 311 (2009) 2933.
[24] Y. Nanishi, Y. Saito, T. Yamaguchi, Japanese Journal of Applied Physics 42 (2003) 2549.
[25] W. Walukiewicz, J.W. Ager III, K.M. Yu, Z. Liliental-Weber, J. Wu, S.X. Li, R.E. Jones, J.D. Denlinger, Journal of Physics D: Applied Physics 39 (2006) R83.
[26] V. Lemos, E. Silveira, J.R. Leite, A. Tabata, R. Trentin, L.M.R. Scolfaro, T. Frey, D.J. As, D. Schikora, K. Lischka, Physical Review Letters 84 (2000) 3666.
[27] R.W. Martin, P.G. Middleton, K.P. O'Donnell, W. Van der Stricht, Applied Physics Letters 74 (1999) 263.
[28] Y.H. Huang, C.L. Cheng, T.T. Chen, Y.F. Chen, K.T. Tsen, Journal of Applied Physics 101 (2007) 103521.
[29] G.B. Stringfellow, Journal of Crystal Growth 312 (2010) 735.
[30] M. Pristovsek, J. Stellmach, M. Leyer, M. Kneissl, Physica Status Solidi (c) 6 (2009) S565.
[31] R.A. Oliver, M.J. Kappers, C.J. Humphreys, G.A.D. Briggs, Journal of Crystal Growth 272 (2004) 393.
[32] S.B. Che, T. Shinada, T. Mizuno, X. Wang, Y. Ishitani, A. Yoshikawa, Japanese Journal of Applied Physics 45 (2006) L1259.